# UT-SEA: A Compact High-Power Prismatic Series Elastic Actuator

Nicholas Paine and Luis Sentis
Department of Mechanical Engineering
The University of Texas at Austin
Austin, Texas 78712
npaine@mail.utexas.edu, lsentis@austin.utexas.edu

***Abstract*—This paper discusses design and control of a prismatic series elastic actuator (SEA) with high power density in a small and lightweight form factor. We propose a design that pushes the performance boundary of electrical SEAs by using motor over-volting techniques coupled with a highly efficient drivetrain to enable large continuous actuator force while retaining speed. Compact size is obtained through the use of a novel piston-style ballscrew support mechanism and a concentrically placed compliant element. Model-based controllers maximize both force and position control performance of a bench top UT-SEA powered joint with a nonlinear mechanical linkage. We use these controllers to demonstrate the high speed, large displacement position tracking performance of the actuator.**

## I. Introduction

Series Elastic Actuation (SEA) is a departure from the traditional approach of rigid actuation commonly used in factory room robotics. Unlike rigid actuators, SEAs contain an elastic element in series with the mechanical energy source. The elastic element gives SEAs several performance benefits compared to rigid actuation including high force fidelity (by measuring elastic deformation), low mechanical impedance, tolerance to impact loads, and the opportunity for mechanical energy storage [1], [2]. However, SEAs have much lower resonant frequencies than their rigid counterparts, thus reducing achievable system bandwidth.

Motor-driven SEAs have been widely used in the fields of legged robotics and human orthotics [3]. The design of each motor-driven SEA (abbreviated "SEA" for the rest of the paper) contains a motor, a speed reduction, a compliant element, and a power transmission to route mechanical power to the joint. There are many different possible implementations for each of these SEA elements, each with its advantages and disadvantages. [4], [5], [6] propose rotary designs based primarily on commercially available off-the-shelf (COTS) parts, using a planetary gearbox for reduction, rotary or compression springs as the compliant element, and power transmission through a bevel gear [6] or chain/cable [4], [5]. Other designs opt to use more compact rotary actuators based on backlash-free harmonic drives for the reduction and compact high-rigidity custom planar springs [7], [8]. [9] also uses a harmonic drive but chooses lower stiffness die/compression springs to increase potential energy storage with one degree of freedom being driven remotely by a chain. [10] uses a novel worm-gear/rotary-spring/spur-gear design which allows the motor to be placed orthogonally to the joint axis at the cost of reduced efficiency and non-backdrivability due to the worm gear. [11], [12], [13] propose prismatic designs which use highly efficient and backlash-free ballscrews as the primary reduction followed by a cable drive to allow the actuator to remotely drive a revolute joint. [11] includes a belt drive between the motor and the ballscrew to allow for an additional speed reduction. Finally, [14] uses a ballscrew but directly drives the joint with a pushrod style drive.

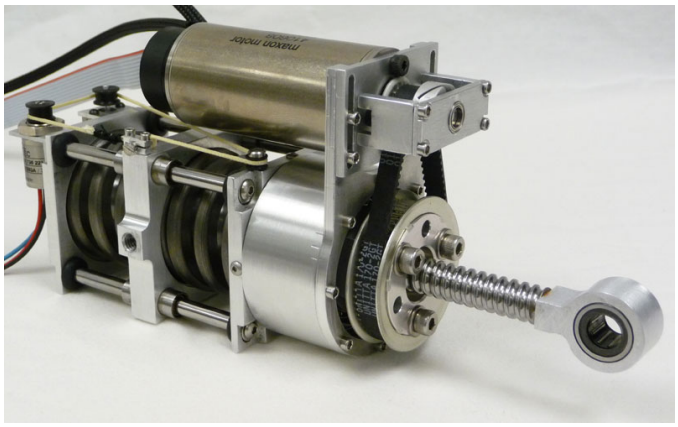

Fig. 1. University of Texas Series Elastic Actuator (UT-SEA).

Variable stiffness actuators extend the SEA concept by adding an additional degree of freedom which is capable of mechanically adjusting the passive elastic stiffness [15], [16], [17], [18]. Other SEA implementations have experimented with non-linear spring stretching to maximize energy storage [19].

This paper highlights research in development of a compact, light-weight, high-power actuator designed to enable energetic and high speed locomotion in electrically actuated legged systems (Figure 1). The design and control challenges associated with this goal include studies in energy transfer from a power source, through a motor, drivetrain, and mechanical actuator dynamics, to the actuated joint efficiently and in a controlled manner. These challenges are addressed with contributions in high-voltage motor interfacing for increased actuator torque and an efficient, power-dense mechanical design. We present intelligent model-based controllers designed to maximize both

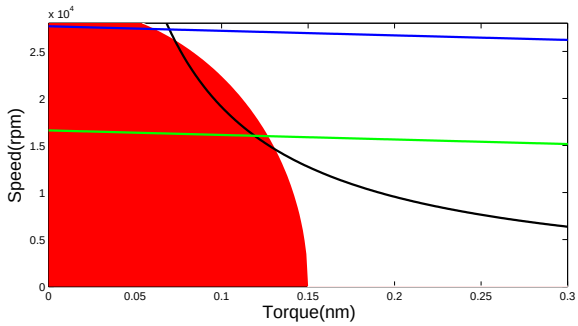


Fig. 2. Motor operating range for Maxon EC-powermax 30 as taken from the datasheet. The red area is an approximation of the thermally permissible continuous operating region. The black line shows the motor's rated mechanical power (200W). A motor is capable of operating inside of the area below the speed-torque curve for a given applied voltage. The green line is the speed-torque curve for Vmax=48V while the blue line shows the speed-torque curve for Vmax=80V.

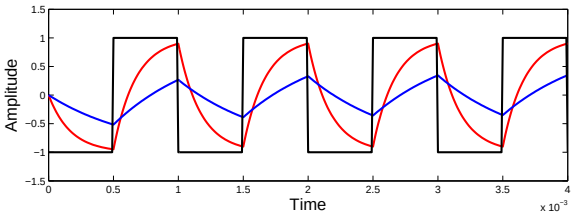


Fig. 3. PWM current control. The black line represents the PWM voltage signal applied to the motor. Motor over-volting causes the amplitude of current peaks to increase (red line). Adding series inductance increases the R-L time constant and lowers current peaks to safer levels (blue line).

tracking accuracy and bandwidth. Finally, we present experimental results showing real-world performance of the full system.

## II. Design

We began design with a set of loose performance specifications (peak joint torques around 70Nm and maximum velocities around 15 rad/sec) obtained from simulations of legged locomotion in rough terrain and discussions with other designers in the field. These values can easily be changed to target alternate performance specifications due to the highly dimensional space of the UT-SEA design parameters.

### A. Motor

After a comparison of motors from several different vendors, we selected a Maxon EC-powermax 30 BLDC to power to our actuator due to its high power-to-weight ratio. This motor is rated at 48 volts, but is capable of much higher speed (maximum motor speed is proportional to voltage as shown in Figure 2). By increasing source voltage from 48 volts to 80 volts, achievable motor speed is increased from 16600 rpm to 27600 rpm.

Motor over-volting must be approached carefully. A motor may be modeled as an R-L circuit in series with a speed-dependent voltage source. Current control mode amplifiers

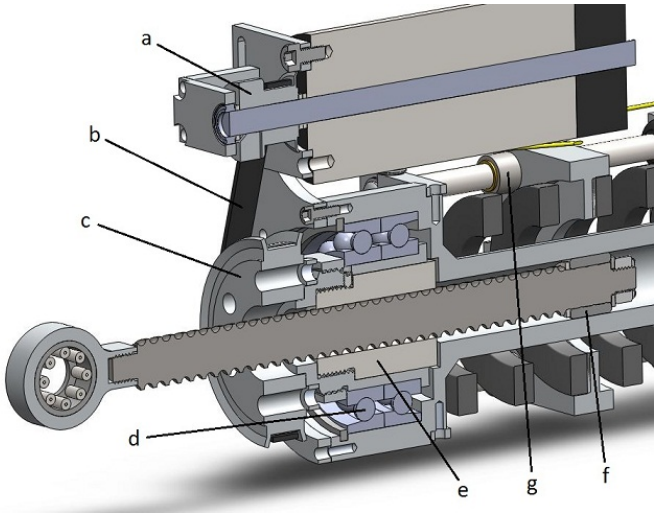


Fig. 4. Cross section of the UT-SEA showing drivetrain components including: (a) small pulley (b) GT style belt (c) large pulley (d) angular-contact bearings (e) ballnut (f) piston-style ballscrew support (g) miniature ball bearing guides.

control current through this circuit using high-frequency pulse-width-modulated (PWM) voltage. The PWM frequency must be much faster than the R-L circuit time constant to limit current oscillations (see Figure 3). Higher oscillation amplitude increases RMS current through the motor which can lead to overheating. To address these issues we chose a motor amplifier with a fast PWM frequency (Elmo Ocarina 15/100) and placed high current inductors in series with each motor phase to increase the inductance seen by the amplifier. Calculations indicated that a series inductance of at least 0.082mH would ensure current loop stability.

The high motor speed provided by over-volting enables the use of a large speed reduction which increases both intermittent and continuous torque capability compared to designs with lower voltages and lower speed reductions. A large reduction scales maximum speed without intrinsically decreasing dynamic performance since acceleration depends on inertia, which is reduced from the load to the motor by $1/N^2$ for an $N$ reduction.

### B. Drivetrain

To maximize mechanical power at the joint, energy must be transmitted from the motor to the joint with as few losses as possible. We chose a pulley/ballscrew reduction design similar to [11] for several reasons. A pulley/ballscrew reduction is efficient (typically above 90%), shock resistant, backdrivable while the pulley ratio reduces the high motor speed to a speed more suitable for driving the ballscrew.

Unlike other SEA designs, our design drives the ballnut instead of the ballscrew ([20] uses a similar ballnut-driven design but is a non-series-elastic cable-driven actuator). Driving the ballnut enables two features which help reduce the size and weight of the UT-SEA. First, ballscrew support is incorporated directly into the actuator housing using an innovative piston-

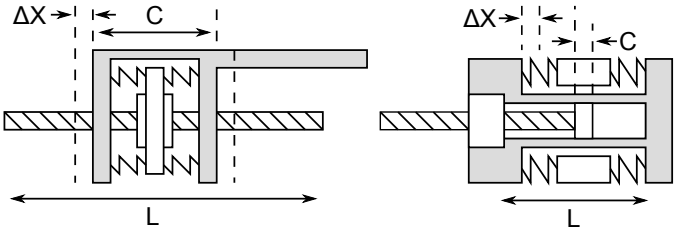


Fig. 5. Range of motion comparison between conventional prismatic actuators (left) and the UT-SEA design (right). $L$ is ballscrew travel length, $C$ is the effective carriage length, and $\Delta X$ is maximum spring deflection. Using these terms, range of motion for both configurations is equal to $L-2\Delta X-C$, but the conventional SEA suffers from a much larger $C$.

style guide (see figure 4). This feature replaces the long, bulky rails used to support the output carriage in conventional prismatic SEA design. Secondly, the compliant element is placed concentrically around the piston-style ballscrew support which gives series elasticity without adding to the length of the actuator.

The ballnut is supported by dual angular contact bearings which allow the ballnut to rotate within the housing while transmitting axial force from the ballnut to the housing. Custom preloaded die springs (manufactured by Diamond Wire Spring Co.) transmit force from the actuator housing to the chassis ground. The die springs are supported by four miniature ball bearing guide rails (Misumi) which are mounted to the housing using grommets that allow for slight misalignment during operation. The miniature ball bearing guides offer both lower friction and higher tolerance to torsional loads than bushing style guides. Force sensing is measured using a 20,000 CPR incremental encoder (Avago AEDA 3300) along with an absolute sensor (Novotechnik Vert-X 1302) to remove the need for startup calibration. A low stretch, low creep Vectran cable is attached to the chassis ground and is routed using pulleys and an idler around the two spring deflection sensors.

### C. Spring Placement and Stiffness

Placing the spring between the motor housing and the chassis ground instead of between the motor output and the load ([11] refers to this style of SEA as "Force Sensing Compliant (FSC) Actuation") leads to several tradeoffs. FSC style actuators have the advantage of being more compact since the compliant element does not have to travel with the load but may be placed statically behind the actuator (or it can be remotely located as shown in [9]). Prismatic FSCs also have greater range of motion for a given ballscrew travel length compared to prismatic SEAs as shown in Figure 5. The primary drawback of FSCs is that they do not allow control of output force using motor position. For SEAs, output force is equal to $k(x_{load} - x_{motor})$ which turns force control into a motor position control problem. For FSCs output force is equal to $kx_{housing}$. Because $x_{housing}$ is coupled to $x_{motor}$ through the dynamics of the actuator and the load, it cannot easily be controlled by motor position.

Spring stiffness was chosen to maximize energy storage. For a given force, soft springs are able to store more energy than stiff springs. Peak force, desired deflection (maximum possible deflection to minimize stiffness), and the geometric constraints of the actuator were given as design specifications to Diamond Wire Spring Co. The result was a spring with a stiffness rate of 138 N/mm which effectively doubles to 277 N/mm for the actuator spring constant since two springs are used with precompression. Experiments using this spring rate yield a small signal closed loop force bandwidth of approximately 18Hz as shown in section III.

TABLE I
UT-SEA DESIGN PARAMETERS

| | |
|---|---|
| Weight | 1168 g |
| Stroke | 6 cm |
| Max Speed | 32.5 cm/sec |
| Continuous Force | 848 N |
| Intermittent Force | 2800 N |
| Spring Stiffness | 277.78 N/mm |
| Force Resolution | 0.31 N |
| Operating Voltage | 80 V |

The end result of design is a pushrod FSC-style SEA that is compact enough to be placed at each joint of an articulated leg. Such small size enables a modular leg design similar to those seen in hydraulically actuated robots ([21], [22]). Articulated leg designs using linear actuators benefit from the nonlinear linkage kinematics created at the joint (see Figure 8). Torque generated by such a linkage has an angle dependent moment arm which can be used to place high torque and high speed capability where they are needed (high torque during leg bending, high speed during leg extension). A summary of the design parameters for the actuator can be seen in table I.

## III. MODELING AND CONTROL

Legged systems experience periods of high output impedance during stance phase and low output impedance during swing phase. A class of controllers that takes advantage of this discrepancy is Raibert-style controllers which use force control during stance phase and position control during swing phase [23]. This strategy suggests that actuators for legged systems should be capable of controlling both output force and position.

### A. Force Control

A common approach to control the force generated by a SEA is by controlling either position or velocity of the motor to track some desired spring deflection [6], [24], [25]. However, as previously mentioned, FSC style actuators cannot be controlled in this manner because of the location of the spring between the actuator housing and chassis ground. Instead, output force must be controlled using motor torque directly. In the static case output force of the UT-SEA ($F_o$) depends only on motor torque ($\tau_m$) and is parameterized by pulley reduction ($N_p$) drivetrain efficiency ($\eta$) and ballscrew lead ($l$).

$$N = \frac{F_o}{\tau_M} = \frac{2\pi N_p \eta}{l} \tag{1}$$

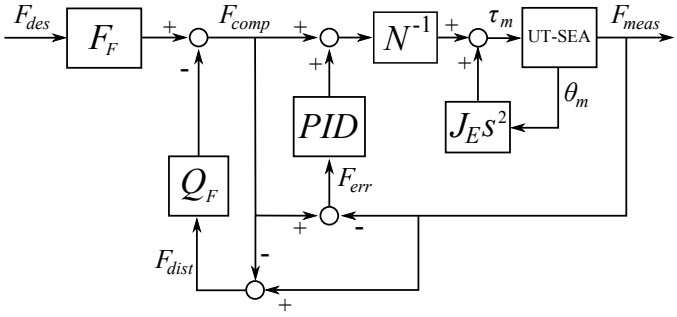


Fig. 6. Block diagram of the control structure used for force control. The notations represent: $N$: the speed reduction from the motor to the output, $J_E$: extended motor inertia used to compensate for motor dynamics.

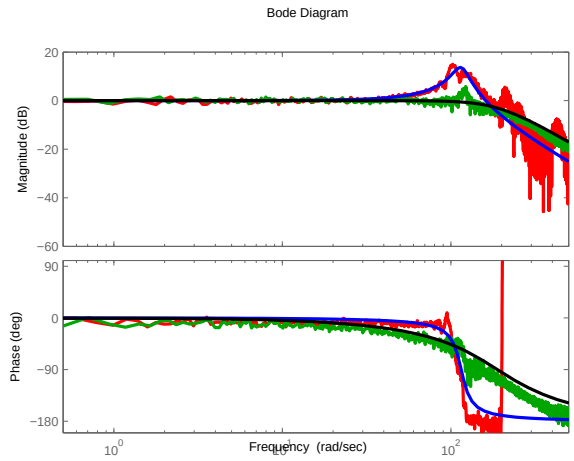


Fig. 7. Frequency response of two force controllers and their respective models. The red/blue curves show force control with no knowledge of the actuator dynamics while the green/black curves show an improved response with much lower resonance using a controller with dynamic compensation ($F_F$). Small signal closed loop force bandwidth is approximately18Hz.

Inspired by [10], our force controller uses equation 1 as a feedforward term combined with PID feedback, motor dynamics compensation, and a simple disturbance observer (figure 6). The motor dynamics compensation improves high-frequency tracking performance while the disturbance observer, combined with a low pass filter ($Q_F$, $f_c$ = 1HZ), removes steady state error.

Experimental analysis of the frequency response of this controller clearly identifies its second order response profile which was then fitted to a mass-spring-damper model (figure 7). A dynamic compensation filter ($F_F$, $f_c$ = 30Hz) is added to the input of the force controller to remove resonant frequencies in the response using model inversion.

$$F_F = LPF \cdot (s^2 m + sb + k) \tag{2}$$

### B. Position Control

Fast, stable position control is crucial for high speed legged locomotion. A model-based position controller can accelerate and decelerate leg mass smoothly and quickly even for large changes in desired position.

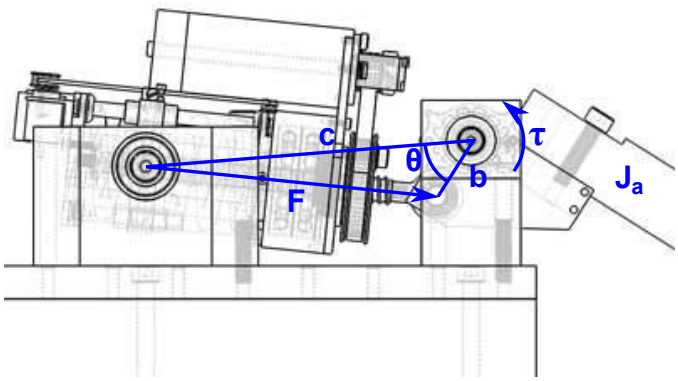


Fig. 8. UT-SEA mounted on a test bench with the prismatic linkage geometry shown. The notations represent: $c$: distance between the actuator pivot and the arm pivot, $b$: distance between the arm pivot and the push rod pivot, $F$: actuator force, $\tau$: torque exerted on the output arm, $J_a$: inertia of the output arm.

Figure 8 shows the kinematic representation of the UT-SEA mounted to drive a rotary joint. Actuator force $F$ generates output torque $\tau$ according to the following equation:

$$\tau = F \frac{cb \sin\theta}{\sqrt{b^2 + c^2 - 2bc\cos\theta}} \tag{3}$$

The dynamics relating effective torque to output angle are

$$\tau = J_a \ddot{\theta} + B_a \dot{\theta} + \tau_g \tag{4}$$

where $\tau_g$ is the torque due to gravity and is parameterized by the mass of the output link ($m_a$), the distance from the point of rotation to the center of mass ($l_m$) and an angle ($\phi$) to correct for $c$ not being orthogonal to the gravity vector:

$$\tau_g = -m_a g l_m \cos(\theta + \phi) \tag{5}$$

Combining (3) (4) and (5) the full dynamics from actuator force to output angle are then represented by the following nonlinear differential equation:

$$F = \frac{\sqrt{b^2 + c^2 - 2bc\cos\theta}}{cb\sin\theta}(J_a\ddot{\theta} + B_a\dot{\theta} - m_a g l_m \cos(\theta + \phi)) \tag{6}$$

Our position control approach first considers the simple problem of controlling output angle given a torque: $\tau = J_a\ddot{\theta} + B_a\dot{\theta}$. This problem is easily solved using model inversion with a low pass filter ($f_c$ = 20Hz) which yields a compensator $F_p$:

$$F_p = LPF \cdot (J_a s^2 + B_a s) \tag{7}$$

The resulting torque signal can then be gravity compensated by adding eq. 5. Multiplying this signal by the inverse of the nonlinear kinematics (equation 3) converts desired torque into

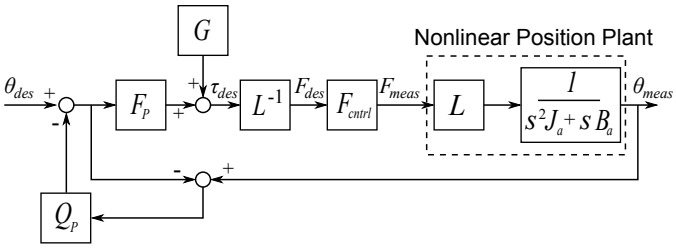


Fig. 9. Block diagram of the control structure used for position control. The notations represent: $G$: gravity compensation torque, $L$: nonlinear linkage kinematics, $F_{cntrl}$: the force control block shown in figure 6.

desired actuator force. This desired force is then passed to the force controller as can be seen in Figure 9.

Without some form of feedback the position controller would not be able to track a desired position due to modeling error and external disturbances. A disturbance observer resolves this issue by treating tracking error as model disturbance and feeding the error through a low pass filter ($f_c$ = 20Hz) and back into the position control loop.

## IV. Experimental Results

Experiments were performed on a PC-104 form factor computer from Advanced Digital Logic (ADLS15PC) running Ubuntu Linux with an RTAI patched kernel to enable real time computation. Force control was performed at 1kHz while position control was performed at 500Hz. Data was passed to and from the actuator using analog and quadrature signals which pass through a custom signal conditioning board. We developed two auxiliary systems to aid in testing the actuator. One system was used to measure spring stiffness versus displacement (see Figure 11) to accurately determine the stiffness of the springs received from the manufacturer. The second system was uses to test misalignment tolerance for a variety of linear guides including miniature ball bearing guides and bushing style guides.

To simulate high speed swing-phase style position tracking, we used a chirp signal with a peak-to-peak amplitude of 30 degrees and a maximum frequency of 2.5Hz (Figure 12). While the measured arm angle follows the reference signal closely, position overshoot develops at frequencies above 1Hz. We believe this is primarily due to backlash that developed in the system after a control input error caused excessively high forces. This backlash reduces the performance of the inner force control loop and also hinders position control. A video submitted with this paper shows the high-speed position tracking experiment.

By plotting the speed/torque points of operation during the high speed position tracking experiment (Figure 13) it is clear how the UT-SEA benefits from higher operating voltage.

## V. Conclusions and Future Work

This paper introduced the UT-SEA, a compact, light-weight, high-power actuator designed to empower the next generation of electrically actuated legged machines. Unlike other prismatic SEAs, the UT-SEA features a tightly integrated pushrod

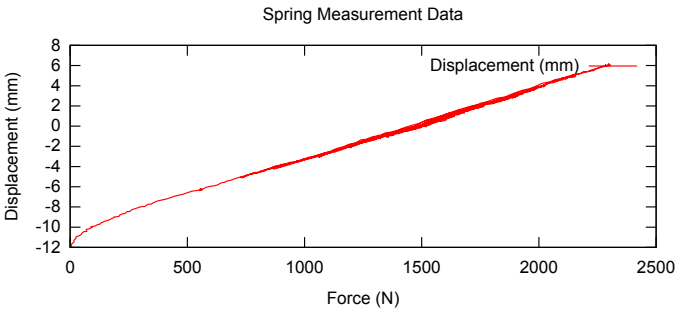


Fig. 10. Spring measurement data. A curve fit was applied to the data the from F=1000N to F=2000N to obtain an accurate spring constant.

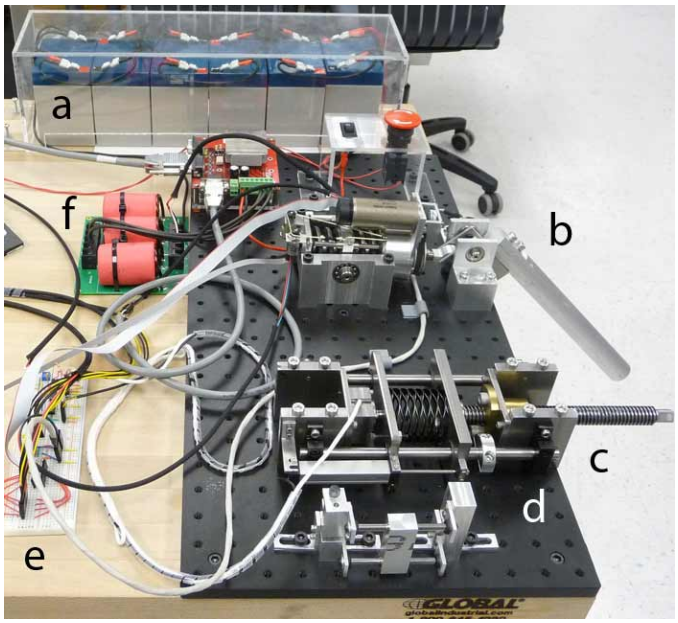


Fig. 11. Experimental setup includes (a) a bank of six 12V lead acid batteries connected in series to deliver 80V (b) the UT-SEA actuator attached to the rotary joint (c) spring measurement system (d) a system used to compare various linear guide mechanisms (e) signal conditioning (f) oversized series inductance (300uH as compared to the required 82uH).

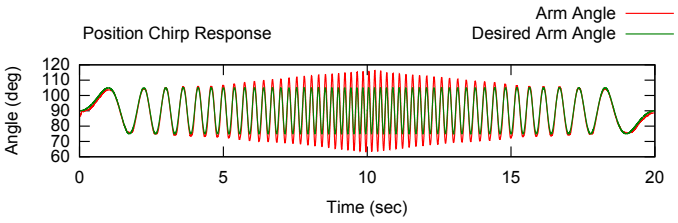


Fig. 12. Position reference tracking for a chirp input signal from zero to 2.5Hz using a 30 degree peak-to-peak amplitude. The only load applied is the arm mass (0.387 kg).

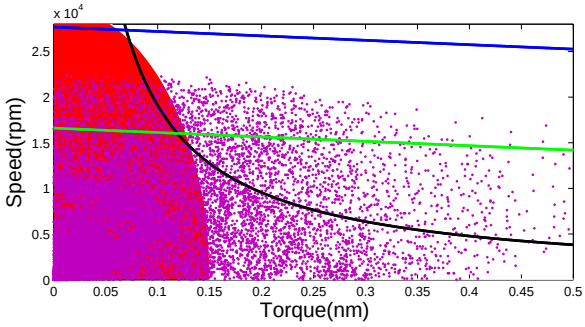


Fig. 13. Motor operating capability overlaid with operating points from high speed position tracking sampled at 1kHz. Points above the green line would be unattainable with a design using a 48 volt supply.

design which enables the actuator to be housed within a robotic leg and use a nonlinear mechanical linkage to drive a rotary joint. High motor voltage and current filtering enable the use of a large speed reduction which significantly increases both continuous and peak torque capabilities. Placement of the elastic element between the actuator housing and chassis ground creates a design with increased range of motion and compactness. Controllers are designed to leverage knowledge of the mechanical properties of the actuator to improve signal tracking accuracy and dynamic response.

Experiments with the UT-SEA are still at an early stage. Full performance characteristics such as maximum output power and torque, operating efficiency, and maximum system bandwidth all need to be studied in greater detail. Additionally, comparisons with other types of control methods will indicate if there is additional performance that can be attained. Small changes can be made to the mechanical design which will improve maintainability, ease of assembly, and remove sensor cable slip. In the future we hope to experiment with higher degrees of freedom to study problems such as jumping, passive energy storage, and task space control.

## REFERENCES


[1] G. Pratt and M. Williamson, "Series elastic actuators," in *Intelligent Robots and Systems 95. 'Human Robot Interaction and Cooperative Robots', Proceedings. 1995 IEEE/RSJ International Conference on*, vol. 1, aug 1995, pp. 399 –406 vol.1.

[2] S. Arumugom, S. Muthuraman, and V. Ponselvan, "Modeling and application of series elastic actuators for force control multi legged robots," *Journal of Computing*, vol. 1, 2009.

[3] J. Pestana, R. Bobin, J. C. Arevalo, and E. Garcia Armada, "Characterization of emerging actuators for empowering legged robots," in *CLAWAR*, 2010.

[4] S. Curran and D. Orin, "Evolution of a jump in an articulated leg with series-elastic actuation," in *Robotics and Automation, 2008. ICRA 2008. IEEE International Conference on*, may 2008, pp. 352 –358.

[5] M. Hutter, C. Remy, and R. Siegwart, "Design of an articulated robotic leg with nonlinear series elastic actuation," in *Proc. of The 12th International Conference on Climbing and Walking Robots and the Support Technologies for Mobile Machines (CLAWAR)*, September 2009, pp. 645–652.

[6] K. Kong, J. Bae, and M. Tomizuka, "Control of rotary series elastic actuator for ideal force-mode actuation in human-robot interaction applications," *Mechatronics, IEEE/ASME Transactions on*, vol. 14, no. 1, pp. 105 –118, feb. 2009.

[7] C. Lagoda, A. Schouten, A. Stienen, E. Hekman, and H. van der Kooij, "Design of an electric series elastic actuated joint for robotic gait rehabilitation training," in *Biomedical Robotics and Biomechatronics (BioRob), 2010 3rd IEEE RAS and EMBS International Conference on*, sept. 2010, pp. 21 –26.

[8] M. Diftler, J. Mehling, M. Abdallah, N. Radford, L. Bridgwater, A. Sanders, R. Askew, D. Linn, J. Yamokoski, F. Permenter, B. Hargrave, R. Piatt, R. Savely, and R. Ambrose, "Robonaut 2 - the first humanoid robot in space," in *Robotics and Automation (ICRA), 2011 IEEE International Conference on*, may 2011, pp. 2178 –2183.

[9] M. Hutter, C. Remy, M. Hoepflinger, and R. Siegwart, "Scarleth: Design and control of a planar running robot," in *Proc. of the IEEE/RSJ International Conference on Intelligent Robots and Systems (IROS)*, 2011.

[10] K. Kong, J. Bae, and M. Tomizuka, "A compact rotary series elastic actuator for knee joint assistive system," in *Robotics and Automation (ICRA), 2010 IEEE International Conference on*, may 2010, pp. 2940 –2945.

[11] A. Edsinger-Gonzales and J. Weber, "Domo: a force sensing humanoid robot for manipulation research," in *Humanoid Robots, 2004 4th IEEE/RAS International Conference on*, vol. 1, nov. 2004, pp. 273 – 291 Vol. 1.

[12] P. Gregorio, M. Ahmadi, and M. Buehler, "Design, control, and energetics of an electrically actuated legged robot," *Systems, Man, and Cybernetics, Part B: Cybernetics, IEEE Transactions on*, vol. 27, no. 4, pp. 626 –634, aug 1997.

[13] J. Pratt and G. Pratt, "Intuitive control of a planar bipedal walking robot," in *Robotics and Automation, 1998. Proceedings. 1998 IEEE International Conference on*, vol. 3, may 1998, pp. 2014 –2021 vol.3.

[14] D. Robinson, J. Pratt, D. Paluska, and G. Pratt, "Series elastic actuator development for a biomimetic walking robot," in *Advanced Intelligent Mechatronics, 1999. Proceedings. 1999 IEEE/ASME International Conference on*, 1999, pp. 561 –568.

[15] J. Hurst, J. Chestnutt, and A. Rizzi, "The actuator with mechanically adjustable series compliance," *Robotics, IEEE Transactions on*, vol. 26, no. 4, pp. 597 –606, aug. 2010.

[16] T.-H. Huang, J.-Y. Kuan, and H.-P. Huang, "Design of a new variable stiffness actuator and application for assistive exercise control," in *Intelligent Robots and Systems (IROS), 2011 IEEE/RSJ International Conference on*, sept. 2011, pp. 372 –377.

[17] N. G. Tsagarakis, I. Sardellitti, and D. G. Caldwell, "A new variable stiffness actuator (compact-vsa): Design and modelling," in *Intelligent Robots and Systems (IROS), 2011 IEEE/RSJ International Conference on*, sept. 2011, pp. 378 –383.

[18] M. Grebenstein, A. Albu-Schaffer, T. Bahls, M. Chalon, O. Eiberger, W. Friedl, R. Gruber, S. Haddadin, U. Hagn, R. Haslinger, H. Hoppner, S. Jorg, M. Nickl, A. Nothhelfer, F. Petit, J. Reill, N. Seitz, T. Wimbock, S. Wolf, T. Wusthoff, and G. Hirzinger, "The dlr hand arm system," in *Robotics and Automation (ICRA), 2011 IEEE International Conference on*, may 2011, pp. 3175 –3182.

[19] I. Thorson and D. Caldwell, "A nonlinear series elastic actuator for highly dynamic motions," in *Intelligent Robots and Systems (IROS), 2011 IEEE/RSJ International Conference on*, sept. 2011, pp. 390 –394.

[20] P. Garrec, "Design of an anthropomorphic upper limb exoskeleton actuated by ball-screws and cables," in *Scientific Bulletin, Series D*, vol. 72, no. 2, 2010.

[21] M. Raibert, K. Blankespoor, G. Nelson, R. Playter, and T. B. Team, *BigDog, the Rough-Terrain Quadruped Robot*, 2008, pp. 10 822–10 825. [Online]. Available: http://www.df.unibo.it/divulgazione/attualita/bigdog.pdf

[22] C. Semini, N. Tsagarakis, E. Guglielmino, and D. Caldwell, "Design and experimental evaluation of the hydraulically actuated prototype leg of the hyq robot," in *Intelligent Robots and Systems (IROS), 2010 IEEE/RSJ International Conference on*, oct. 2010, pp. 3640 –3645.

[23] M. H. Raibert, *Legged Robots That Balance*. Cambridge, Mass: MIT Press, 1986.

[24] H. Vallery, R. Ekkelenkamp, H. van der Kooij, and M. Buss, "Passive and accurate torque control of series elastic actuators," in *Intelligent Robots and Systems, 2007. IROS 2007. IEEE/RSJ International Conference on*, 29 2007-nov. 2 2007, pp. 3534 –3538.

[25] G. Wyeth, "Demonstrating the safety and performance of a velocity sourced series elastic actuator," in *Robotics and Automation, 2008. ICRA 2008. IEEE International Conference on*, may 2008, pp. 3642 –3647.